

# Effect of Substrate Coupling on the Performance and Variability of Monolayer MoS<sub>2</sub> Transistors

Abdullah Alharbi<sup>✉</sup>, Student member, IEEE, Zhujun Huang, Takashi Taniguchi, Kenji Watanabe, and Davood Shahrjerdi<sup>✉</sup>, Senior Member, IEEE

**Abstract**— We study the effect of substrate coupling on the variability and the device characteristics of monolayer MoS<sub>2</sub> field-effect transistors (FETs). Our electrical measurement results reveal significant improvements of key FET device metrics and marked reduction of device variability with reducing the interfacial energy. We attribute the observed improvements of the device characteristics to the reduction of the interface trap density and the suppression of the charged impurity scattering. This study establishes the critical role of substrate coupling on the performance and variability of monolayer MoS<sub>2</sub> FETs.

**Index Terms**— MoS<sub>2</sub>, variability, interfacial energy, FET.

## I. INTRODUCTION

MATERIALS discovery and device innovations underlie the advances of the semiconductor industry. A recent example of such research activities includes exploring device prospects of 2-D transition metal dichalcogenides (TMDs), [1], [2]. However, key to the implementation of a realistic electronic system from these nanomaterials is the ability to reliably produce high performance devices with homogeneous electrical properties. Achieving this goal requires a fundamental understanding of the variability in TMD devices.

Past studies have established that stray charges in the surrounding environment, e.g., oxide substrates, are major sources of variability in devices made of nanomaterials. Therefore, various approaches have been implemented for mitigating the device variability, including reducing the oxide thickness [3], [4], using clean fabrication processes [4], [5], and capping nanomaterials with an impermeable film [6]–[8]. Whereas the critical role of oxide substrates on the variations of the device performance is generally accepted, no study has yet examined this problem by studying the adhesion energy at the interface between a 2-D TMD and an oxide substrate. We refer to this energy as the interfacial energy.

Here, we investigate the effect of substrate coupling on the electrical characteristics of MoS<sub>2</sub> transistors. To do so, we fabricated and analyzed four groups of four-point back-gated FETs, where each group represents an interfacial energy that is distinct from the other groups.

Manuscript received October 31, 2018; accepted November 22, 2018. Date of publication November 28, 2018; date of current version January 9, 2019. This work was supported in part by NSF under Grant ECCS-1638598 and Grant MRI-1531664 and in part by the Gordon and Betty Moore Foundation under Grant GBMF 4838. The review of this letter was arranged by Editor Z. Chen. (*Corresponding author: Davood Shahrjerdi.*)

A. Alharbi, Z. Huang, and D. Shahrjerdi are with the Department of Electrical and Computer Engineering, New York University, Brooklyn, NY 11201 USA (e-mail: davood@nyu.edu).

T. Taniguchi and K. Watanabe are with the National Institute of Materials Science, Ibaraki 305-0044, Japan.

Color versions of one or more of the figures in this letter are available online at <http://ieeexplore.ieee.org>.

Digital Object Identifier 10.1109/LED.2018.2883808

## II. EXPERIMENT

In our study, we used as-grown monolayer MoS<sub>2</sub> films as the starting material, where MoS<sub>2</sub> was grown using chemical vapor deposition (CVD) on a silicon substrate covered with 285 nm of SiO<sub>2</sub> [9], [10]. In our initial experiments, we found that the as-grown MoS<sub>2</sub> cannot be detached from the substrate by using a standard polymeric stamp [11]. This observation agrees with a previous study by Na *et al.*, reporting the strong adhesion of the as-grown MoS<sub>2</sub> films to the SiO<sub>2</sub> growth substrate [12]. Also similar to their report, our x-ray photoelectron spectroscopy (XPS) measurements (spot size of 10 μm) of the as-grown films (Fig. 1k) showed no detectable covalent or ionic bonding between MoS<sub>2</sub> and SiO<sub>2</sub>, thereby suggesting that the bonding at the interface primarily originates from van der Waals interactions. Although the physical origin of this strong adhesion is still unknown, the remarkably high van der Waals force at the MoS<sub>2</sub>-SiO<sub>2</sub> interface has been attributed to the high growth temperature [12].

Therefore, to produce MoS<sub>2</sub> with weaker adhesion to SiO<sub>2</sub>, we developed a new gold-assisted layer transfer process, described in section II-A. We show in section II-B that these transferred layers have the smallest interfacial energy among the three device groups that were fabricated on SiO<sub>2</sub>. Past studies suggest that annealing can lead to stronger bonding between TMD films and the substrate [13]–[15]. Therefore, to create a third set of devices with an intermediate interfacial energy, we did layer transfer of the as-grown monolayer MoS<sub>2</sub> films followed by annealing at 250 °C for 30 minutes under ultra-high vacuum (UHV; 2 × 10<sup>-10</sup> torr). This annealing condition has been shown to maintain the MoS<sub>2</sub> film quality [16]. From now, we refer to these three groups of samples as S-I (as-grown), S-II (transferred and then UHV-annealed), and S-III (as-transferred).

### A. Device fabrication

To fabricate FETs, we first selected 10 triangular monolayer MoS<sub>2</sub> films at random from four different growth runs. The monocrystalline structure of triangular films allows us to exclude the possible role of grain boundaries on the variations of the device characteristics. Next, we used a combination of electron-beam lithography (EBL), metal evaporation, and lift-off to create three rectangular gold (Au) islands of similar size within each triangular film. We then performed a second EBL step using PMMA resist to create openings that are slightly larger than the Au islands, followed by etching the exposed MoS<sub>2</sub> in a CF<sub>4</sub>/O<sub>2</sub> plasma. Figs. 1a–c show the top-view illustration, the cross-section schematic, and an example top-view optical image of an MoS<sub>2</sub> film after these two steps.

To construct the S-II and S-III device sets, we transferred two islands from each MoS<sub>2</sub> film to two different corners

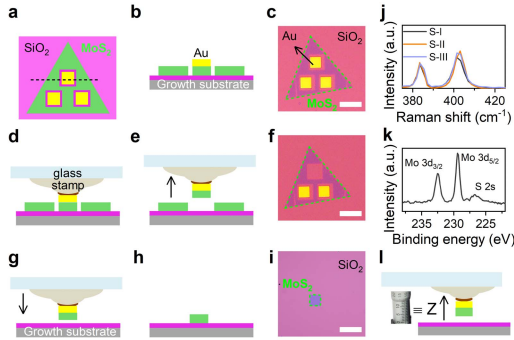


**Fig. 1.** (a) Top-view illustration, (b) cross-section schematic, and (c) optical image depicting Au-MoS<sub>2</sub> islands within a monolayer flake on SiO<sub>2</sub>. (d)-(f) We developed a process based on a stamp-assisted transfer technique for detaching the as-grown MoS<sub>2</sub> from SiO<sub>2</sub>. (g) The detached Au-MoS<sub>2</sub> islands were placed in predefined regions of the substrate, followed by (h)-(i) chemical removal of Au. (j) Representative Raman spectra of MoS<sub>2</sub> on the samples S-I, S-II, and S-III. (k) XPS spectrum of an as-grown CVD MoS<sub>2</sub>. (l) We estimated the energy release rate by measuring the displacement  $Z$ , which is the vertical distance it takes to detach a Au-MoS<sub>2</sub> island from the substrate during a transfer process. Scale bars are 20  $\mu\text{m}$ .

of the same substrate, where no MoS<sub>2</sub> growth had originally occurred. To do so, we developed a new process based on a stamp-assisted transfer technique. In particular, our approach uses a thin-film (20 nm) Au as an intermediate layer between the stamp and MoS<sub>2</sub>. We chose Au for two reasons. First, it provides strong binding to the sulfur-based materials, on the order of 1 eV [17]. The second reason is the ease of its processing and chemical etching. Figs. 1d-e show the process steps for detaching a Au-MoS<sub>2</sub> island from the substrate. Our results confirmed that the stack of stamp-Au-MoS<sub>2</sub> can overcome the strong adhesion between the as-grown MoS<sub>2</sub> and SiO<sub>2</sub> (Fig. 1f). The detached islands were then placed at predefined regions of the same substrate, allocated to S-II or S-III devices (Fig. 1g). Fig. 1j shows the equivalency of the Raman data among the S-I, S-II, and S-III device groups.

After the placement, the Au layer was removed chemically (Transene), shown in Figs. 1h-i. We then cleaved the substrate into three pieces to create the S-I, S-II, and S-III samples. The S-II sample was then annealed in a UHV to enhance the adhesion between the transferred MoS<sub>2</sub> layers and SiO<sub>2</sub>. Forming Au electrodes using a combination of EBL, metal evaporation, and lift-off completed the device fabrication. Fig. 2a shows the schematic illustration and an example optical image of a back-gated MoS<sub>2</sub> FET on SiO<sub>2</sub>.

Past research has shown that h-BN substrates can significantly reduce the long-range Coulomb scattering (and hence increase the carrier mobility) in a variety of 2-D channel materials [18]–[20]. The h-BN substrates achieve this by decoupling the channel material from the oxide substrate. Therefore, to examine the case where MoS<sub>2</sub> is fully decoupled from the SiO<sub>2</sub> substrate, we fabricated a fourth group of devices (S-IV) by transferring CVD MoS<sub>2</sub> islands onto mechanically exfoliated h-BN flakes. Apart from the step involving the stacking of the MoS<sub>2</sub> islands onto h-BN, the other fabrication steps of the S-IV devices were identical to those described above. Fig. 2b shows the schematic illustration and an example optical image of a back-gated FET on h-BN.

### B. Estimation of interfacial energy

To gain insight into the effect of the substrate coupling on the device performance, we quantified the adhesion energy

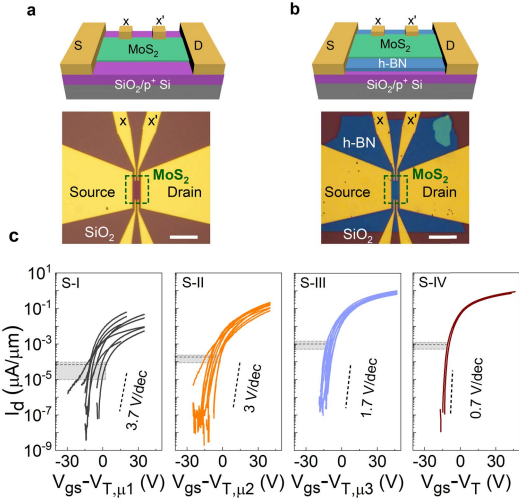


**Fig. 2.** Schematic and optical image of MoS<sub>2</sub> FETs (a) on SiO<sub>2</sub> and (b) on h-BN substrates. Scale bars are 10  $\mu\text{m}$ . (c) Transfer characteristics of a few tens of FETs measured at  $V_{\text{ds}} = 100$  mV. Notice the increase of the ON current, reduction of SS, and improvement of the device consistency from S-I to S-IV. The gray shading represents the upper and lower bounds of  $I_{\text{FB}}$  within each device group.

**TABLE I**  
SUMMARY OF MEASURED  $Z$  AND ESTIMATED NORMALIZED  $G$

Sample ID	Experiment	Average $Z$ ( $\mu\text{m}$ )	Normalized $G$
S-I	As-grown	162	1
S-II	Transfer + UHV anneal	108	0.45
S-III	As-transferred	52	0.1
S-IV	Transferred onto h-BN	N.A.	N.A.

at the MoS<sub>2</sub>-SiO<sub>2</sub> interface. The interfacial energy  $\gamma$  is given by the product of the energy release rate ( $G$ ) and the bond density. Since the bond density is the same among all samples in our experiments, we used  $G$  as a proxy for  $\gamma$ . We estimated  $G$  using the formulation derived from the single-beam cantilever technique [21]  $G = (3Eh^3Z^2)/(8L^4)$  where  $Z$ ,  $E$ ,  $L$ , and  $h$  denote the vertical displacement, Young's modulus of the film, beam length, and thickness. The beam theory is commonly used for estimating the surface energy of solid-state materials [21] and also for estimating the adhesion energy between 2-D materials and their growth substrates [12], [22]. To simplify the analysis, we kept the dimensions of the MoS<sub>2</sub> islands and the substrate thickness the same in all transfer experiments. This allowed us to quantitatively compare the magnitude of the energy release rate for S-I, S-II, and S-III simply by comparing their corresponding vertical displacement. Table I summarizes the average measured  $Z$  of each device set and the corresponding normalized  $G$ , which was calculated by taking the ratio of the average  $Z$  for each device set to that of S-I. We measured the vertical displacement (with an accuracy of 5  $\mu\text{m}$ ) using the micromanipulator in our layer transfer setup (Fig. 1l), and averaged over four transfer experiments. Our calculations revealed that the interfacial energy of the as-transferred MoS<sub>2</sub> is about 10 times smaller than the as-grown film.

### III. RESULTS AND DISCUSSION

In Fig. 2c, we show the transfer characteristics of a few tens of FETs from our device groups. All FETs had the same gate length of 3  $\mu\text{m}$ . From the data, we observed that the ON current, SS, and the device-to-device variations

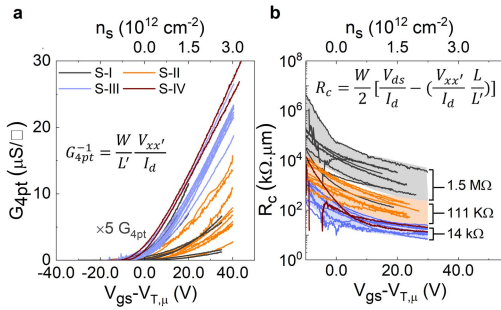


**Fig. 3.** (a) Comparison of  $G_{4pt}$ . For better illustration,  $G_{4pt}$  of S-I was multiplied by a factor of 5. The inset shows the equation for calculating  $G_{4pt}$ .  $W$ ,  $L'$ , and  $V_{xx'}$  denote channel width, spacing, and voltage drop between the  $x$  and  $x'$  electrodes. (b) We found  $R_c$  from the four-point measurements.  $n_s$  is the charge density calculated from  $C_{ox}(V_{gs} - V_T)$ .

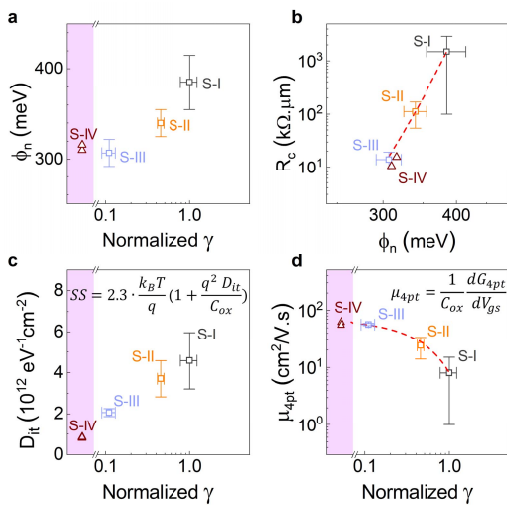


**Fig. 4.** (a) We observed the lowering of  $\phi_n$  with reducing the interfacial energy.  $\phi_n$  was estimated from  $I_{FB}$  in Fig. 2c. (b) The exponential relationship between  $R_c$  and  $\phi_n$  agrees with the barrier-limited nature of contacts in MoS<sub>2</sub> FETs. (c) Summary of  $D_{it}$  estimated from the SS data in Fig. 2c. (d) Four-point measurements also revealed significant increase of the carrier mobility with reducing the interfacial energy. The pink shading in all plots represents the region where MoS<sub>2</sub> is on h-BN.

improved noticeably with reducing the interfacial energy and approaching those of FETs on h-BN. These results clearly illustrate the critical role of the adhesion energy at the MoS<sub>2</sub>-SiO<sub>2</sub> interface on the device performance and variability.

Next, to illustrate the reasons for the observed improvements of the ON current, we performed four-point measurements. The intrinsic channel conductivity  $G_{4pt}$  was measured using the voltage drop between  $x$  and  $x'$  terminals ( $V_{xx'}$ ) when biasing the source and drain contacts (Fig. 2). The specific contact resistance  $R_c$  was calculated by subtracting the intrinsic channel resistance ( $(G_{4pt} \times L'/L)^{-1}$ ) from the total resistance ( $V_{ds}/I_d$ ) [19]. Fig. 3a-b show the summary of  $G_{4pt}$  and  $R_c$  for all FETs. The data indicate that the observed improvement of the ON current with decreasing the interfacial energy is due to the simultaneous increase of the channel conductivity and the reduction of the contact resistance.

To explain the observed reduction of  $R_c$ , we estimated the true Schottky barrier height ( $\phi_n$ ) using the thermionic emission model. The predictions of this model have been shown to be consistent with  $\phi_n$  extracted from the Arrhenius technique [23]. To estimate  $\phi_n$ , we first determined the flat

band current ( $I_{FB}$ ) from the transfer characteristics of the FETs in Fig. 2c. Specifically,  $I_{FB}$  corresponds to the point at which the sub-threshold characteristics begin to deviate from the exponential trend. The gray shading in each plot represents the upper and lower bounds of  $I_{FB}$  for each device group. We then estimated  $\phi_n$  by comparing the experimental  $I_{FB}$  data against the theoretical predictions given by [23]

$$I_{FB} = q \int_{\phi_n}^{\infty} M(E - \phi_n) f(E) dE \quad (1)$$

where  $f(E)$  and  $M(E)$  represent the Fermi-Dirac distribution function and the number of modes per unit width. Specifically,  $\phi_n$  was used as a variable in Eq. 1 to match the experimental and theoretical  $I_{FB}$ . Fig. 4a shows the summary of the extracted  $\phi_n$ . From the data, we found that  $\phi_n$  decreased with the reduction of the interfacial energy. Moreover, the exponential relationship between  $R_c$  and  $\phi_n$  in Fig. 4b is consistent with the barrier-limited behavior of contacts in MoS<sub>2</sub> FETs [23]–[26], indicating that the reduction of  $\phi_n$  was the main cause for the observed improvements of  $R_c$ .

It is currently unclear why reducing the interfacial energy caused the reduction of  $\phi_n$ . Notably, this trend coincided with the reduction of the trap density ( $D_{it}$ ) at the interface of MoS<sub>2</sub> and SiO<sub>2</sub>, Fig. 4c. In this plot, we calculated  $D_{it}$  from the SS of FETs [27]. On the basis of this observation, we speculate that the interactions between vacancy defects in MoS<sub>2</sub> and oxygen atoms in SiO<sub>2</sub> underlie the apparent variations of  $\phi_n$  with the interfacial energy. This picture is consistent with further decrease of  $D_{it}$  when MoS<sub>2</sub> FETs were fabricated on h-BN substrates. However, the physical principles that govern this effect should yet be elucidated.

To better illustrate the trend of how the device variability changed with the interfacial energy, we made the distribution plots for each device parameters (not shown). The data points and the error bars in Fig. 4 represent the mean value and the variance, extracted from those distribution plots. As can be seen, reducing the interfacial energy significantly diminished the variability in FET device performance.

Lastly, we examined the effect of the interfacial energy on the carrier mobility ( $\mu_{4pt}$ ) from the four-point data. The data suggest significant increase (about a factor of 7) of  $\mu_{4pt}$  with decreasing the interfacial energy (Fig. 4d). Moreover, the data show that, with reducing the interfacial energy, the mobility of FETs on SiO<sub>2</sub> substrates approaches those on h-BN. It is well-established that the use of h-BN substrates suppresses the long-range Coulomb scattering originating from the charged impurities in the oxide substrate [18]. Therefore, we infer that the reduction of the interfacial energy has a similar effect on the carrier transport in MoS<sub>2</sub> FETs fabricated on SiO<sub>2</sub>.

#### IV. CONCLUSION

This study provides an experimental evidence for the critical effect of the substrate coupling on the performance and variability of 2-D TMD devices. Our results establish that reducing the interfacial energy can remarkably improve device characteristics and their consistency. This finding provides an important practical guide for engineering TMD growth and fabrication processes on oxide substrates.

#### ACKNOWLEDGMENT

This research used resources of the Center for Functional Nanomaterials, which is a U.S. DOE Office of Science Facility, at Brookhaven National Laboratory under Contract No. DE-SC0012704.

## REFERENCES

- [1] D. Akinwande, N. Petrone, and J. Hone, "Two-dimensional flexible nanoelectronics," *Nature Commun.*, vol. 5, Dec. 2014, Art. no. 5678, doi: [10.1038/ncomms6678](https://doi.org/10.1038/ncomms6678).
- [2] S. Manzeli, D. Ovchinnikov, D. Pasquier, O. V. Yazyev, and A. Kis, "2D transition metal dichalcogenides," *Nature Rev. Mater.*, vol. 2, Jun. 2017, Art. no. 17033, doi: [10.1038/natrevmats.2017.33](https://doi.org/10.1038/natrevmats.2017.33).
- [3] Q. Cao, S.-J. Han, A. V. Penumatcha, M. M. Frank, G. S. Tulevski, J. Tersoff, and W. E. Haensch, "Origins and characteristics of the threshold voltage variability of quasiballistic single-walled carbon nanotube field-effect transistors," *ACS Nano*, vol. 9, no. 2, pp. 1936–1944, Sep. 2015, doi: [10.1021/nn506839p](https://doi.org/10.1021/nn506839p).
- [4] K. K. H. Smithe, S. V. Suryavanshi, M. M. Rojo, A. D. Tedjarati, and E. Pop, "Low variability in synthetic monolayer MoS<sub>2</sub> devices," *ACS Nano*, vol. 11, no. 8, pp. 8456–8463, 2017, doi: [10.1021/acsnano.7b04100](https://doi.org/10.1021/acsnano.7b04100).
- [5] K. Kang, S. Xie, L. Huang, Y. Han, P. Y. Huang, K. F. Mak, C.-J. Kim, D. Müller, and J. Park, "High-mobility three-atom-thick semiconducting films with wafer-scale homogeneity," *Nature*, vol. 520, no. 7549, pp. 656–660, 2015, doi: [10.1038/nature14417](https://doi.org/10.1038/nature14417).
- [6] A. D. Franklin, G. S. Tulevski, S.-J. Han, D. Shahrjerdi, Q. Cao, H.-Y. Chen, H.-S. P. Wong, and W. Haensch, "Variability in carbon nanotube transistors: Improving device-to-device consistency," *ACS Nano*, vol. 6, no. 2, pp. 1109–1115, 2012, doi: [10.1021/nn203516z](https://doi.org/10.1021/nn203516z).
- [7] D. Shahrjerdi, A. D. Franklin, S. Oida, J. A. Ott, G. S. Tulevski, and W. Haensch, "High-performance air-stable n-type carbon nanotube transistors with erbium contacts," *ACS Nano*, vol. 7, no. 9, pp. 8303–8308, May 2013, doi: [10.1021/nn403935v](https://doi.org/10.1021/nn403935v).
- [8] S. Rahimi, R. Ghosh, S. Kim, A. Dodabalapur, S. Banerjee, and D. Akinwande, "The positive effects of hydrophobic fluoropolymers on the electrical properties of MoS<sub>2</sub> transistors," *Appl. Sci.*, vol. 6, no. 9, p. 236, 2016, doi: [10.3390/app6090236](https://doi.org/10.3390/app6090236).
- [9] A. Alharbi, P. Zahl, and D. Shahrjerdi, "Material and device properties of superacid-treated monolayer molybdenum disulfide," *Appl. Phys. Lett.*, vol. 110, no. 3, p. 033503, 2017, doi: [10.1063/1.4974046](https://doi.org/10.1063/1.4974046).
- [10] A. Alharbi, D. Armstrong, S. Alharbi, and D. Shahrjerdi, "Physically unclonable cryptographic primitives by chemical vapor deposition of layered MoS<sub>2</sub>," *ACS Nano*, vol. 11, no. 12, pp. 12772–12779, 2017, doi: [10.1021/acsnano.7b07568](https://doi.org/10.1021/acsnano.7b07568).
- [11] A. Castellanos-Gomez, M. Buscema, R. Molenaar, V. Singh, L. Janssen, H. S. J. van der Zant, and G. A. Steele, "Deterministic transfer of two-dimensional materials by all-dry viscoelastic stamping," *2D Mater.*, vol. 1, no. 1, p. 011002, 2014, doi: [10.1088/2053-1583/1/1/011002](https://doi.org/10.1088/2053-1583/1/1/011002).
- [12] S. R. Na, Y. Kim, C. Lee, K. M. Liechti, and J. W. Suk, "Adhesion and self-healing between monolayer molybdenum disulfide and silicon oxide," *Sci. Rep.*, vol. 7, Nov. 2017, Art. no. 14740, doi: [10.1038/s41598-017-14921-9](https://doi.org/10.1038/s41598-017-14921-9).
- [13] L. Su, Y. Yu, L. Cao, and Y. Zhang, "Effects of substrate type and material-substrate bonding on high-temperature behavior of monolayer WS<sub>2</sub>," *Nano Res.*, vol. 8, no. 8, pp. 2686–2697, 2015, doi: [10.1007/s12274-015-0775-1](https://doi.org/10.1007/s12274-015-0775-1).
- [14] K. Jin, D. Liu, and Y. Tian, "Enhancing the interlayer adhesive force in twisted multilayer MoS<sub>2</sub> by thermal annealing treatment," *Nanotechnology*, vol. 26, no. 40, p. 405708, 2015, doi: [10.1088/0957-4484/26/40/405708](https://doi.org/10.1088/0957-4484/26/40/405708).
- [15] W. Xu, D. Kozawa, Y. Liu, Y. Sheng, K. Wei, V. B. Koman, S. Wang, X. Wang, T. Jiang, M. S. Strano, and J. H. Warner, "Determining the optimized interlayer separation distance in vertical stacked 2D WS<sub>2</sub>:hBN:MoS<sub>2</sub> heterostructures for exciton energy transfer," *Small*, vol. 14, no. 13, p. 1703727, Mar. 2018, doi: [10.1002/smll.201703727](https://doi.org/10.1002/smll.201703727).
- [16] H.-J. Kim, D. Kim, S. Jung, M.-H. Bae, S. N. Yi, K. Watanabe, T. Taniguchi, S. K. Chang, and D. H. Ha, "Homogeneity and tolerance to heat of monolayer MoS<sub>2</sub> on SiO<sub>2</sub> and h-BN," *RSC Adv.*, vol. 8, no. 23, p. 12900–12906, 2018, doi: [10.1039/C8RA01849A](https://doi.org/10.1039/C8RA01849A).
- [17] E. Pensa, E. Cortést, G. Corthey, P. Carro, C. Vericat, M. H. Fonticelli, G. Benítez, A. A. Rubert, and R. C. Salvarezza, "The chemistry of the sulfur–gold interface: In search of a unified model," *Accounts Chem. Res.*, vol. 45, no. 8, pp. 1183–1192, 2012, doi: [10.1021/ar200260p](https://doi.org/10.1021/ar200260p).
- [18] C. R. Dean, A. F. Young, I. Meric, C. Lee, L. Wang, S. Sorgenfrei, K. Watanabe, T. Taniguchi, P. Kim, K. L. Shepard, and J. Hone, "Boron nitride substrates for high-quality graphene electronics," *Nature Nanotechnol.*, vol. 5, pp. 722–726, Aug. 2010, doi: [10.1038/NNANO.2010.172](https://doi.org/10.1038/NNANO.2010.172).
- [19] H. C. P. Movva, A. Rai, S. Kang, K. Kim, B. Fallahazad, T. Taniguchi, K. Watanabe, E. Tutuc, and S. K. Banerjee, "High-mobility holes in dual-gated WSe<sub>2</sub> field-effect transistors," *ACS Nano*, vol. 9, no. 10, pp. 10402–10410, 2015, doi: [10.1021/acsnano.5b04611](https://doi.org/10.1021/acsnano.5b04611).
- [20] X. Cui, G.-H. Lee, Y. D. Kim, G. Arete, P. Y. Huang, C.-H. Lee, D. A. Chenet, X. Zhang, L. Wang, F. Ye, F. Pizzocchero, B. S. Jessen, K. Watanabe, T. Taniguchi, D. A. Müller, T. Low, P. Kim, and J. Hone, "Multi-terminal transport measurements of MoS<sub>2</sub> using a van der Waals heterostructure device platform," *Nature Nanotechnol.*, vol. 10, no. 6, p. 534–540, 2015, doi: [10.1038/nnano.2015.70](https://doi.org/10.1038/nnano.2015.70).
- [21] R. J. Jaccodine, "Surface energy of germanium and silicon," *J. Electrochem. Soc.*, vol. 110, no. 6, p. 524, 1963, doi: [10.1149/1.2425806](https://doi.org/10.1149/1.2425806).
- [22] T. Yoon, W. C. Shin, T. Y. Kim, J. H. Mun, T.-S. Kim, and B. J. Cho, "Direct measurement of adhesion energy of monolayer graphene as grown on copper and its application to renewable transfer process," *Nano Lett.*, vol. 12, no. 3, pp. 1448–1452, 2012, doi: [10.1021/nl204123h](https://doi.org/10.1021/nl204123h).
- [23] J. Appenzeller, F. Zhang, S. Das, and J. Knoch, "Transition metal dichalcogenide Schottky barrier transistors," in *2D Materials for Nanoelectronics*. Boca Raton, FL, USA: CRC Press, 2016, pp. 207–240, doi: [10.1201/b19623-11](https://doi.org/10.1201/b19623-11).
- [24] A. Allain, J. Kang, K. Banerjee, and A. Kis, "Electrical contacts to two-dimensional semiconductors," *Nature Mater.*, vol. 14, no. 12, pp. 1195–1205, 2015, doi: [10.1038/nmat4452](https://doi.org/10.1038/nmat4452).
- [25] A. Prakash, H. Ilatikhameneh, P. Wu, and J. Appenzeller, "Understanding contact gating in Schottky barrier transistors from 2D channels," *Sci. Rep.*, vol. 7, Oct. 2017, Art. no. 12596, doi: [10.1038/s41598-017-12816-3](https://doi.org/10.1038/s41598-017-12816-3).
- [26] A. Alharbi and D. Shahrjerdi, "Analyzing the effect of high-k dielectric-mediated doping on contact resistance in top-gated monolayer MoS<sub>2</sub> transistors," *IEEE Trans. Electron Devices*, vol. 65, no. 10, pp. 4084–4092, Oct. 2018, doi: [10.1109/TED.2018.2866772](https://doi.org/10.1109/TED.2018.2866772).
- [27] S. Sze and K. K. Ng, *Physics of Semiconductor Devices*. Hoboken, NJ, USA: Wiley, 2006, doi: [10.1002/0470068329](https://doi.org/10.1002/0470068329).